Paper

Iris Recognition System Based on Zak-Gabor Wavelet Packets

Adam Czajka[a] and Andrzej Pacut[a,b]

[a] *Biometric Laboratories, Research and Academic Computer Network NASK, Warsaw, Poland*
[b] *Institute of Control and Computation Engineering, Warsaw University of Technology, Warsaw, Poland*

Abstract—The paper proposes a new iris coding method based on Zak-Gabor wavelet packet transform. The essential component of the iris recognition methodology design is an effective adaptation of the transformation parameters that makes the coding sensitive to the frequencies characterizing ones eye. We thus propose to calculate the between-to-within class ratio of weakly correlated Zak-Gabor transformation coefficients allowing for selection the frequencies the most suitable for iris recognition. The Zak-Gabor-based coding is non-reversible, i.e., it is impossible to reconstruct the original iris image given the iris template. Additionally, the inference about the iris image properties from the Zak-Gabor-based code is limited, providing a possibility to embed the biometric replay attack prevention methodology into the coding. We present the final prototype system design, including the hardware, and evaluate its performance using the database of 720 iris images.

Keywords—biometrics, iris recognition, Zak-Gabor transform.

1. Introduction

Biometric researchers are still looking for the *ideal biometrics*, i.e., both a part of the human body and the applied methodology of its symbolic description fused in one system that is characterized by high usability, produces no errors, is robust with respect to variations of attributes of the human body within a large time scale, immune to diseases, resistant to forgery, and produces no social, religious and ethical objections.

The iris is a complex set of interworking muscles, placed anteriorly to the human eye, thus easy to be observed and measured. It is strongly protected by the cornea and eyelids, minimizing the probability of injuries during human life. The structure of the iris tissue is characterized by high stability over the human life span, high degree of structural richness, and almost neglectful dependence on human genotype [1], allowing for recognizing identical twins. In consequence, iris seems to have all of the attributes we'd like to have in biometrics. This paper presents a new iris recognition methodology, that was used to construct fast, highly reliable and non-invasive biometric system.

2. Iris Images and Their Preprocessing

2.1. Iris Image Capture and Database of Images

Estimation of the method parameters presented in this work are based on proprietary database of 720 iris images, called here further BioBase. The data was collected for 180 different eyes, with 4 images of each eye. We used 3 images of each eye to calculate the iris templates, and the remaining single image of each eye in the verification stage. Images were collected by IrisCUBE camera (Fig. 1) designed and constructed by the authors to capture the iris from a convenient distance, with the desired speed and a minimal user cooperation. The camera has an automatic optics to compensate for small depth-of-field that is typical in iris recognition systems. The IrisCUBE camera implements selected aliveness detection methods [2] to deliver actual biometric samples, what still is not a wide practice in commercial iris acquisition systems. The quality of acquired iris images exceeds the highest quality level specified in ISO standard (marked as 'High' in [3]). Since the hardware used allows for one-eye capture, the images taken may be mutually rotated and the rotation of images used in the estimation stage was corrected using the correlation techniques. The remaining fourth image (used in the verification stage) was not altered and the rotation correction mechanism is inscribed in the recognition methodology.

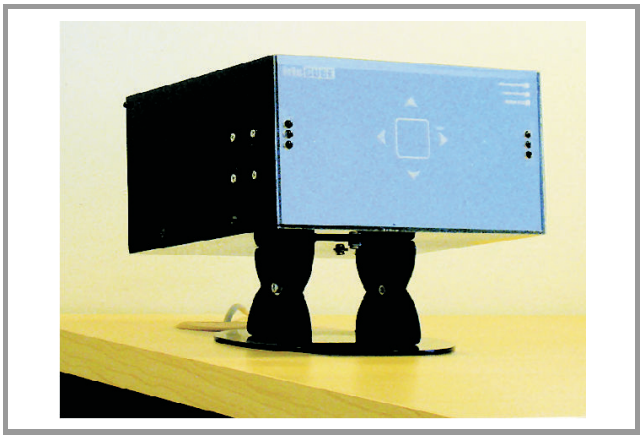

Fig. 1. IrisCUBE camera employed to collect the database used in this work.

2.2. Iris Segmentation

The raw images contain the iris and its surroundings, thus the iris must be first localized. To detect a boundary between the pupil and the iris, we use a method being a specimen of a commonly applied family of methods sensitive to circular dark shapes, and unresponsive to other dark areas as well as light circles, such as specular reflections. Our implementation is based on a modified Hough transform

that employs the image gradient (the so called *directional image*) rather than solely the image gradient value (the so called *edge image*, which neglects the gradient direction). A boundary between the iris and the sclera is approximated by Daugman's integro-differential operator [1] applied to two opposite horizontally placed angular sectors, 45° each, since the entire circular iris boundary may be partially disturbed by eyelids. The two radii of the resulting arcs are averaged to construct a circle approximating the outer iris boundary.

The iris ring limited by the two circular boundaries may still be disrupted by irregular objects like reflections or eyelashes, hence it is desirable to use occlusion detection that does not assume any particular occlusion shape. We thus assess a non-uniformity along the radial direction within the iris ring and then construct map of irregular occlusions. To do so, we first calculate the sample variances of the iris image intensity for a set of radial sectors along entire iris ring. These variances are then compared to the maximum allowed variance obtained for directions in which the probability of iris occlusion is minimal (i.e., set of directions placed horizontally on both sides of the iris ring). Those directions in which the calculated variance exceeds the threshold value is marked as an occlusion direction, and the appropriate occlusion radius is stored.

Based on the localized occlusions, we select two opposite 90° wide angular iris sectors for coding. The experiments (see also [1]) revealed much higher correlation of the iris image in the radial direction as compared to the angular direction, thus each iris sector is transformed by resampling and smoothing to a $P \times R$ rectangle, where $P = 512$ and $R = 16$. The rows f_ℓ of these two rectangles will be further referred to as *iris stripes* (Fig. 2).

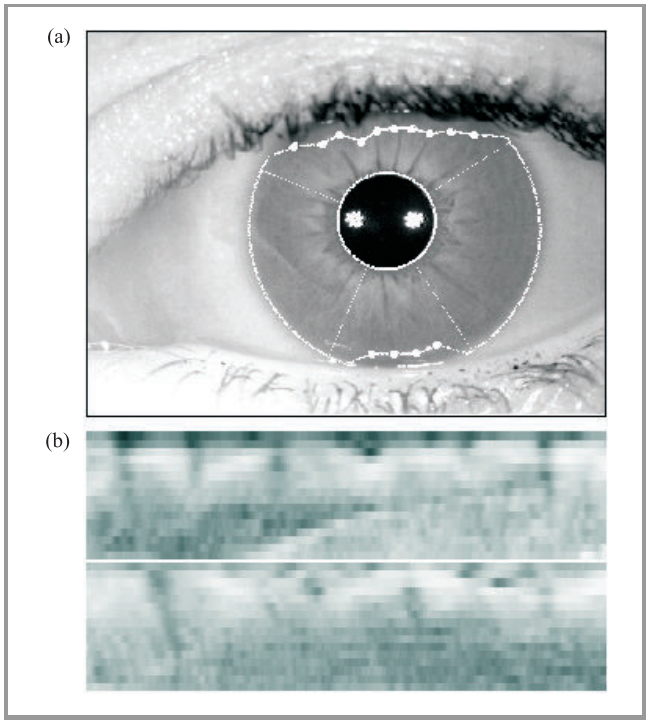

Fig. 2. (a) Raw camera image processed by our system. The eyelids were automatically detected, and the sectors free of occlusions are selected. Star-like shapes on the pupil are reflections of the illumination NIR diodes, and the '+' marks represent the pupil and the iris centers. Full circles correspond to the detected eyelid occlusions. (b) Left and right iris stripes automatically determined for the image shown on (a).

3. Iris Features

3.1. Choice of Features

It is often convenient to characterize a discrete-time signal in the frequency domain, thus describing stationary energy distribution. For non-stationary signals, it might be worthwhile to characterize the frequencies locally, and to find the distribution of signal energy in local (possibly overlapping) time segments by application of *time-frequency* or *time-scale* analysis. Similarly, any constant (time-independent) space-homogeneous 1D or 2D pattern (e.g., image) can be characterized in a 1D or 2D frequency domain using "position" statement instead of "time". If a pattern is not space-homogeneous, its spatial frequency contents may be analyzed locally, with the use of *space-frequency* or *space-scale analysis*. Two important candidates for such analysis are *windowed Fourier transform* (WFT, also called "short time Fourier transform", or STFT) and wavelet transform (WT). Both approaches differ. WFT makes use of window functions constant in size, and frequency shifts are achieved by modulating the window. This property is sometimes at a disadvantage, since for each frequency, the number of cycles inscribed in the analysis window differs, resulting in different averaging horizons for different frequencies. In turn, wavelet analysis achieves frequency shifts by *scaling* the position index. Scaling does not change the number of cycles inscribed into the analysis window, thus providing an even analysis for each frequency. These properties of WFT and WT result in different tilings within the 2D position-frequency plane, namely linear for WFT and logarithmic for WT.

The Gabor transform belongs to WT family, and uses a Gaussian window characterized by its width. The window width significantly influences the resulting iris features and must be carefully chosen. We use the space-frequency analysis that employs waveforms indexed by space, scale and frequency simultaneously, what results in a larger set of possible tilling in the space-frequency plane, possibly redundant. This directs our methodology toward a *wavelet packet* analysis. There is a need to select appropriate frequencies and scales simultaneously to make the transformation sensitive to individual features existing in the iris image. In this paper we propose a systematic selection of appropriate scales and frequencies of the iris coding. Although the iris texture makes a 2D pattern, we simplify it to a set of 1D patterns with a certain loss of information and apply the space-frequency analysis locally to the iris circular sectors to describe their local features and to construct a compact iris features set. This approach enables our method to be applied for databases of images of various resolution.

3.2. Gabor Expansion

Gaussian-shaped windows are not orthogonal (the inner product of any two of all windows is nonzero), therefore Gabor's expansion coefficients cannot be determined in a simple way. Suggested algorithms include making the window function bi-orthonormal to the Gaussian-shaped elementary function and the matrix-based algorithm [4]. However the Gabor's expansion coefficients determination by application of Zak's transform [5] is considered as the fastest method and it is often referred to as Zak-Gabor's transform. In this section we explain briefly the principles of Gabor expansion coefficient calculation through the Zak's transform for one iris stripe and fixed window width. Denote by g_s a one-dimensional Gaussian elementary function of the width index s, sampled at points $0,\ldots,P-1$, namely

$$g_s(p) = e^{-\pi\left((p+\frac{1}{2})/2^s\right)^2}, \quad p = 0,\ldots,P-1, \qquad (1)$$

where $s = 2,3,\ldots,S$, and for the stripe length $P = 512$ we set $S = 8$. If P is (typically) chosen to be even, the $\frac{1}{2}$ term in Eq. (1) makes g_s to be an even function.
Let M be the number of possible translations of g_s, and K be the number of frequency shifts, where, following Bastiaans [5], we always take $M = P/K$. A shifted and modulated version $g_{mk;s}$ of the elementary function g_s can be constructed, namely

$$g_{mk;s}(p) = g_s(p - mK)e^{ikp2\pi/K}, \quad p = 0\ldots P-1, \qquad (2)$$

where $m = 0,\ldots,M-1$ and $k = 0,\ldots,K-1$ denote the space and frequency shifts, respectively, and g_s is wrapped around in the P-point domain. The finite discrete Gabor transform of the iris stripe f_ℓ is defined as a set of complex coefficients $a_{mk;s\ell}$ that satisfy the Gabor signal expansion relationship, namely

$$f_\ell(p) = \sum_{m=0}^{M-1}\sum_{k=0}^{K-1} a_{mk;s\ell}\, g_{mk;s}(p), \quad p = 0\ldots P-1. \qquad (3)$$

Following Bastiaans [5], we further set $K = 2^s$. Note that once the frequency index k is kept constant, $g_{mk;s}$ may be localized in frequency by a modification of s. This is done identically as the scaling in a wavelet analysis, hence we call s the *scale* index. The number of Gabor expansion coefficients $a_{mk;s\ell}$ may be interpreted as the signal's number of degrees of freedom. Note that the number S of scales together with the stripe size P determine both M and K.

3.3. Zak's Transform

The discrete finite Zak transform $\mathscr{Z} f_\ell(\rho,\phi;K,M)$ of a signal f_ℓ sampled equidistantly at P points is defined as the one-dimensional discrete Fourier transform of the sequence $f_\ell(\rho + jK)$, $j = 0,\ldots,M-1$, namely [5]

$$\mathscr{Z} f_\ell(\rho,\phi;K,M) = \sum_{j=0}^{M-1} f_\ell(\rho + jK)e^{-ij\phi 2\pi/M}, \qquad (4)$$

where $M = P/K$. Discrete Zak's transform is periodic both in frequency ϕ (with the period $2\pi/M$) and location ρ (with the period K). We choose ϕ and ρ within the fundamental Zak interval [5], namely $\phi = 0,1,\ldots,M-1$ and $\rho = 0,1,\ldots,K-1$. Similarly to the Fourier transformation, one may reconstruct the original function f_ℓ from its Zak transform by way of the inverse discrete Zak transform, using the following formula

$$f_\ell(\rho + jK) = \frac{1}{M}\sum_{\phi=0}^{M-1} \mathscr{Z} f_\ell(\rho,\phi;K,M)e^{ij\phi 2\pi/M} \qquad (5)$$

and restricting the domain of the results to the fundamental Zak interval.

3.4. Application of Zak's Transform

Application of the discrete Zak transform to both sides of Eq. (3) and rearranging the factors yields

$$\begin{aligned}
&\mathscr{Z} f_\ell(\rho,\phi;K,M) = \\
&= \sum_{j}^{M-1}\left[\sum_{m}^{M-1}\sum_{k}^{K-1} a_{mk;s\ell}\, g_s(\rho + jK - mK)e^{ik\rho 2\pi/K}\right]e^{-ij\phi 2\pi/M} = \\
&= \left[\sum_{m=0}^{M-1}\sum_{k=0}^{K-1} a_{mk;s\ell}e^{-i2\pi(m\phi/M - k\rho/K)}\right]\cdot \\
&\cdot\left[\sum_{j=0}^{M-1} g_s(\rho + jK)e^{-i2\pi j\phi/M}\right] = \\
&= \mathscr{F} a_{s\ell}(\rho,\phi;K,M)\,\mathscr{Z} g_s(\rho,\phi;K,M), \qquad (6)
\end{aligned}$$

where $\mathscr{F} a_{s\ell}[\rho,\phi;K,M]$ denotes the discrete 2D Fourier transform of an array of $a_{s\ell}$ that represents Gabor's expansion coefficients determined for the iris stripe f_ℓ and scale s, and $\mathscr{Z} g_s[\rho,\phi;K,M]$ is discrete Zak's transform of the elementary function g_s.
This shows that Gabor's expansion coefficients can be recovered from the product form Eq. (6). Once K and M are chosen to be powers of 2 (making also the signal length P to be a power of 2), the calculation of both $\mathscr{Z} f[\rho,\phi;K,M]$ and $\mathscr{Z} g[\rho,\phi;K,M]$, and inversion of 2D Fourier series can employ fast Fourier transform thus yielding computation times proportional to those in the FFT.

3.5. Definition of Iris Features

Calculation of Gabor's transform for all iris stripes and for all scales results in a set of coefficients a indexed by the quadruple: within-stripe position, frequency index, scale and stripe index (m,k,s,ℓ). Inspired by Daugman's work [1], we define the signs of the real and imaginary parts of Zak-Gabor coefficients as the feature set $\mathbb{B}$, namely

$$\mathbb{B} = \left\{\mathrm{sgn}(\Re(a_{mk;s\ell})), \mathrm{sgn}(\Im(a_{mk;s\ell}))\right\}, \qquad (7)$$

where: $m = 0,\ldots,M-1$, $k = 0,\ldots,K-1$, $\ell = 0,\ldots,2R-1$ and $s = 2,3,\ldots,S$.

Since the Fourier transform is symmetrical for real signals, for each position m the coefficients with the frequency index $k > K/2$ can be ignored. Since $M = P/K$, for each s there are $(N-1)P/2$ coefficients to be determined. Taking into account that this analysis is carried out for all iris stripes, and remembering that $R = 16$, $S = 8$ and $P = 512$, the total number of coefficients calculated for the iris image is $R(S-1)P = 57,344$. Both real and imaginary parts are coded separately by one bit, hence $N = |\mathbb{B}| = 114,688$ features may be achieved, where $|\cdot|$ denotes the number of elements in a finite set. The features, positioned identically for each iris, may thus form a binary vector. Thus, matching two features requires only a single XOR operation, and the Hamming distance can be applied to calculate the score.

We stress that $\mathbb{B}$ should not be confused with the so called *iriscode*™ invented by Daugman. The latter one is a result of an iris image filtering, while $\mathbb{B}$ is constructed with Gabor expansion coefficients. We now describe how to select a subset of features $\mathbb{B}$ to be included in a final feature set $\mathbb{B}^*$.

3.6. Feature Set Selection

The selection of scales and frequencies of Zak-Gabor coefficients included into the code, and thus selection of the scale s in Eq. (1) and the frequency index k, cannot be guessed *a priori*, due to significant and undetermined iris texture variability. Both parameters are interdependent, have a strong influence on the overall method's efficiency and should be considered simultaneously. Moreover, the full feature set $\mathbb{B}$ is significantly oversized, since it consists of features representing all, possibly inadequate, frequencies of the analyzed image. We thus propose a two-stage method that selects optimal Zak-Gabor based features and can be used to estimate optimal feature set given the quality of iris images. Since only certain subset of $\mathbb{B}$ will be included into the final feature set, all elements of $\mathbb{B}$ will be further referred to as *candidate features*.

Stage one: selection of useful features. The first selection stage consists of choosing a subset $\mathbb{B}^0$ of candidate features $\mathbb{B}$, called here the *useful features*. To determine $\mathbb{B}^0$, we analyze a variability of candidate features.

For each feature b we calculate the *within-eye sum of squares* $SS^W(b)$, and the *between-eye sum of squares* $SS^B(b)$. Intuitively, a feature is *useful* if at least $SS_n^{(W)} < SS_n^{(B)}$. Typically, the number of bits that meet this requirement is still too high (approximately half of bits b_n) and ends up with highly correlated features. We thus introduce a stronger selection mechanisms and categorize features to maximize SS^B and minimize SS^W solving this multicriteria problem by minimizing the distance from the most desired point on $SS^W \times SS^B$ plane. This point was set as $\left(\min_{b\in\mathbb{B}} SS^W(b), \max_{b\in\mathbb{B}} SS^B(b)\right)$, Fig. 3.

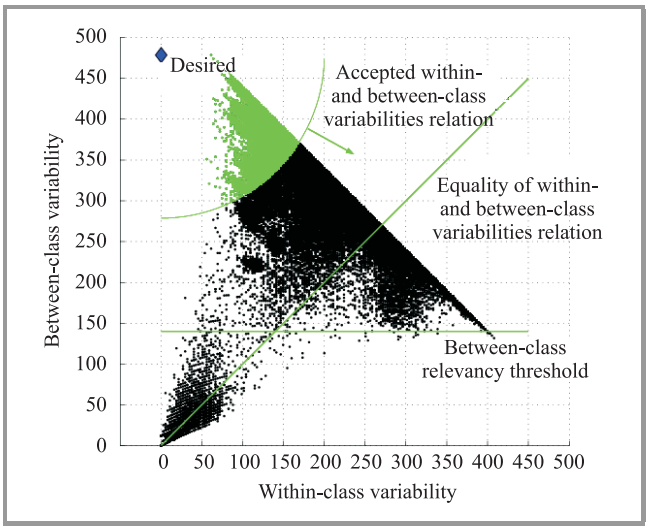

Fig. 3. Within-eye sum of squares versus between-eye sum of squares and the area of *useful features*. Each dot corresponds to real or imaginary part of one Zak-Gabor coefficient. The "desired" point is also marked (we favor coefficients with minimum within-eye and simultaneous maximum between-eye sum of squares).

We use the order introduced by the above procedure in the set of candidate features $\mathbb{B}$ in a procedure removing a high correlation of candidate features to increase an "information density". We include kth candidate feature into the set $\mathbb{B}^0$ only if it is *not strongly correlated* with all the features already selected.

We base our useful feature definition on the *decidability coefficient* d' [1] calculated for a given feature subset. We calculate the decidability coefficient for each set of candidate features included into $\mathbb{B}^0$. The decidability varies with the number of candidate features included: it first grows to reach the maximum and then decreases. Experiments show that the decidability d' is highest for the correlation threshold around 0.3, Fig. 4.

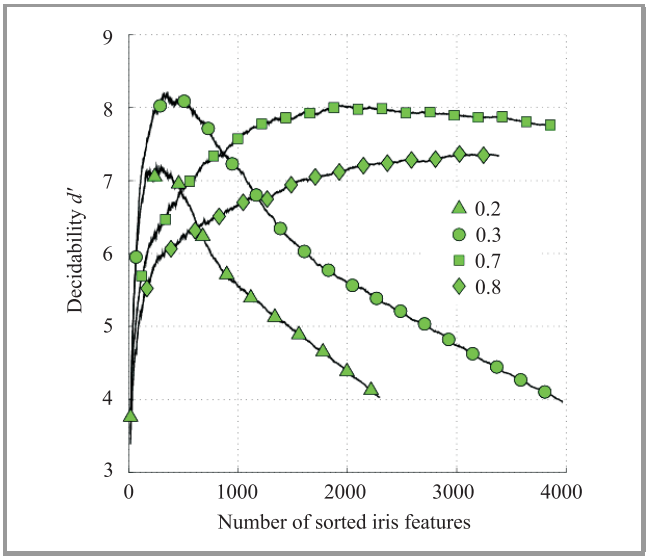

Fig. 4. Decidability coefficient versus number of useful features selected for a few sample correlation coefficients (0.2, 0.3, 0.7 and 0.8) allowed within the *useful features* set.

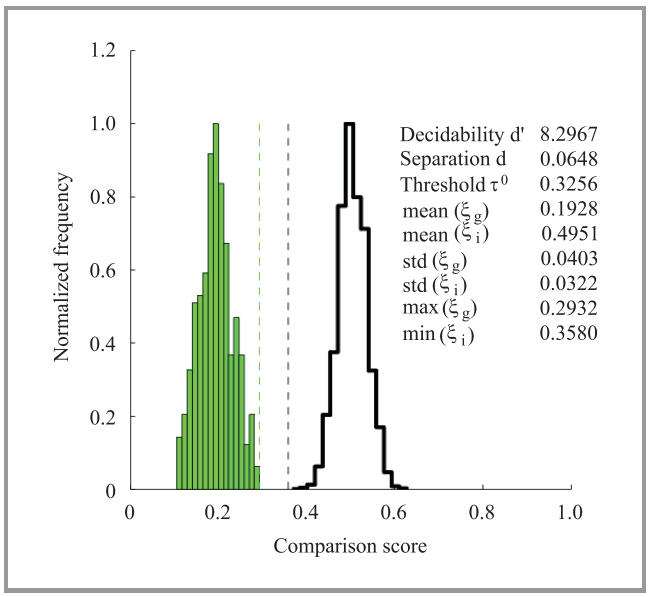

Fig. 5. Score distributions for 360 genuine (left) and 64,440 impostor (right) comparisons, denoted by ξ_g and ξ_i, respectively. Only the useful features $\mathbb{B}^0$ are used. No sample errors were registered for a wide range of acceptance threshold $\tau \in (0.2932, 0.358)$, and in particular for optimal threshold $\tau^0 = 0.3256$.

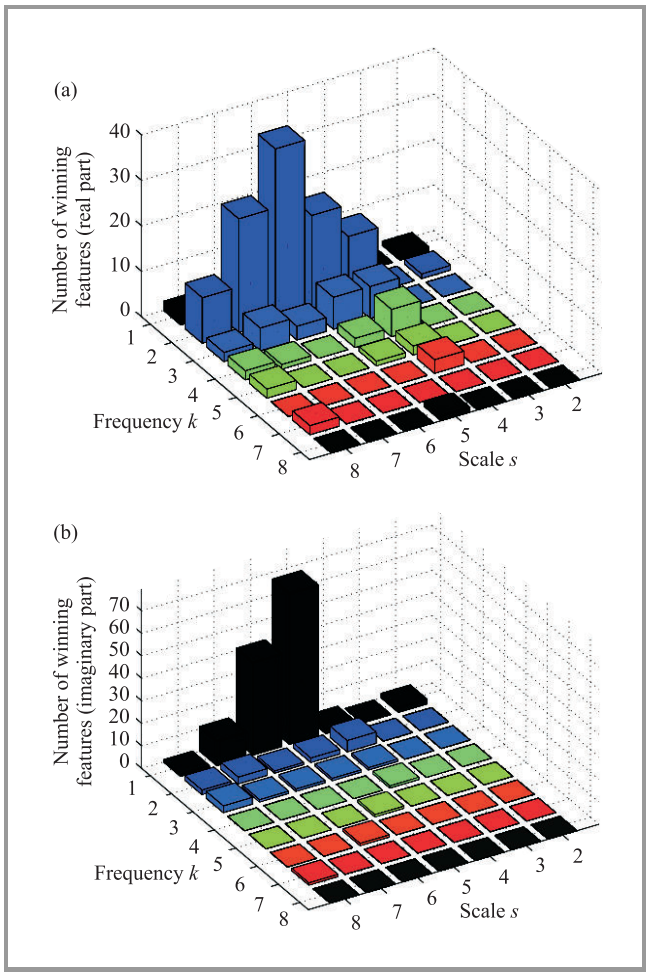

Fig. 6. 2D histogram of how families $\mathbb{B}_{k,s}$ are "populated" by useful features $\mathbb{B}^0$ determined separately for the real (a) and imaginary (b) parts of Zak-Gabor coefficients.

For this solution there is no between-eye – within-eye overlap of sample distributions, i.e., there are no false matches and no false non-match examples in the estimation data set, Fig. 5. The resulting 324 useful features pass to the second feature selection stage. We may add that our procedure included only such features for which $SS^W < SS^B$.

Stage two: selection of feature families. Let $\nu(k,s)$ denote the number of useful features in the *candidate features family* $\mathbb{B}_{k,s}$, which represent all candidate features that are labeled by the same scale k and frequency s, and differ by space indices m and ℓ, namely

$$\mathbb{B}_{k,s} = \{\mathrm{sgn}(\Re(a_{mk;s\ell})), \mathrm{sgn}(\Im(a_{mk;s\ell})) : m = 0,\ldots,M-1, \ell = 0,\ldots,2R-1\}. \quad (8)$$

The higher is $\nu(k,s)$, the more important are the frequency indexed by k and the scale indexed by s in iris recognition. To decide for the best frequencies and scales, independently for real or imaginary parts of the Zak-Gabor coefficients, we sort $\mathbb{B}_{k,s}$ by decreasing $\nu(k,s)$ separately for real and imaginary parts of coefficients. Figure 6 depicts the 'population' of scale-frequency families by winning features $\mathbb{B}^0$. Note that the number of winning features is not identical for all families.

We further prioritize the families that are most frequently 'populated' by the useful features. The sorting rule for families of features mirrors the rule used for useful features selection: we sort $\mathbb{B}_{k,s}$ by the decreasing number of useful features $\mathbb{B}^0$ included in a given family, separately for real and imaginary parts of coefficients. We check the decidability d' and separation d (the difference between maximum genuine score and minimum impostor score, note that $d > 0$ denotes perfect separation between distributions of genuine and impostor scores) and chose the families resulting in maximum d' for a given database, Fig. 7.

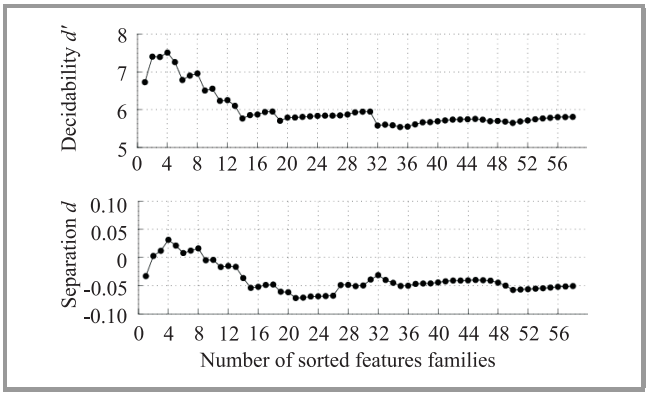

Fig. 7. Decidability d' and separation margin d versus the number of sorted feature families $\mathbb{B}_{k,s}$ included in the feature set.

This rule allows finding the frequency-scale pairs of real and imaginary parts of Zak-Gabor coefficients, which, if chosen as iris features, result in the best separation of distributions of genuine and impostor comparison scores. The feature families set resulting in maximum d' constitutes the *final feature set* $\mathbb{B}^*$, which in our case contains only

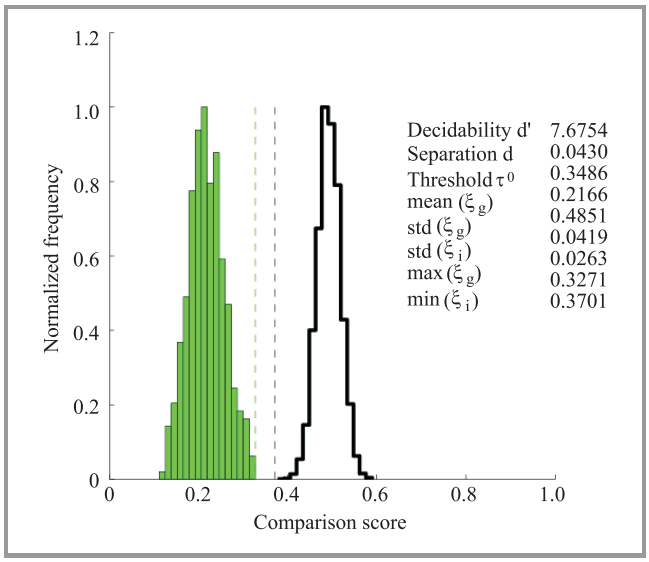

Fig. 8. Same as in Fig. 5, except the selected feature families are used to build the iris feature set. No sample errors are registered for a wide range of acceptance threshold $\tau \in (0.3271, 0.3701)$, and in particular for optimal threshold $\tau^0 = 0.3486$.

four families, what ends up with 1024 bit code. For this final feature set, we still achieved no sample verification errors, Fig. 8.

3.7. Personalize Feature Subsets

Once the optimal feature families, namely the best scale-frequency pairs indexed by s and k, are selected, the iris features set is calculated for those chosen s and k and all $m = 1, \ldots, M-1$, and $\ell = 0, \ldots, 2R-1$. Each Zak-Gabor coefficient can 'measure' the correlation between the modulated Gaussian elementary function $g_{mk;s}$ and the corresponding iris stripe. The question arises how 'robust' are the consecutive Zak-Gabor coefficients against noise, and iris tissue elastic constrictions and dilations.

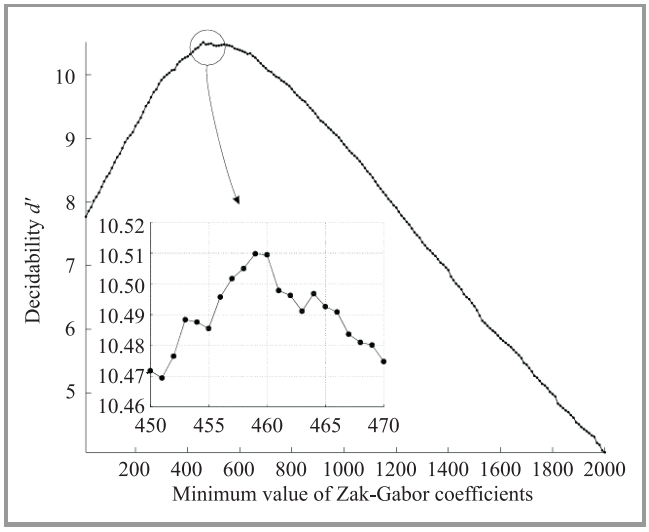

Fig. 9. Decidability versus minimum value of Zak-Gabor coefficients, required to be included in the feature set. For BioBase data, best decidability $d' = 10.5095$ is achieved if using coefficients $a_{mk;s\ell} \geq a^{\text{thr}} = 459$

Due to a significant variability of the iris tissue, some $g_{mk;s}$ may not conform with the iris body, resulting in small coefficients. Such a situation is dangerous, since once the coefficients are close to zero, their signs may depend mostly on a camera noise, and consequently may weaken the final code. This motivates personalization of the iris feature sets that employ only those Zak-Gabor coefficients that exceed experimentally determined threshold a^{thr}, which is the minimum value of Zak-Gabor coefficiens $a_{mk;s\ell}$ required to become a *relevant coefficient* being a base of an iris feature.

To answer the question how big the value of a^{thr} should be, we maximize the decidability d' using a^{thr} as a parameter given a database of iris images. By increasing a^{thr} a greater number of coefficients are neglected. According to observations (Fig. 9) the system reliability first increases, then deteriorates, and the maximum $d' = 10.51$ for $a^{\text{thr}} = 459$ can be found, which is higher than $d' = 7.67$ achieved for a full set of 1024 feature bits (cf. Fig. 8). Although the separation margin d is not increased significantly for the determined a^{thr}, the distribution tails are larger, and the score averages for the comparison of the same and different eyes are spaced more widely compared to non-personalized technique, Fig. 10.

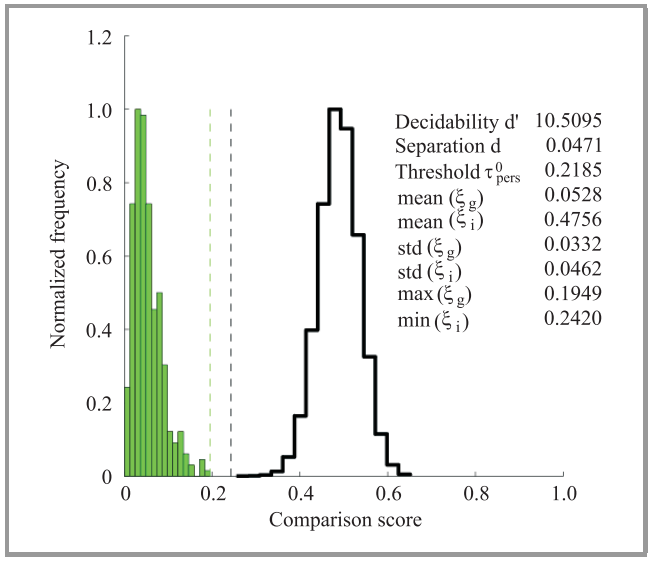

Fig. 10. Same as in Fig. 5, except the personalized features are used for each person, in the way to guarantee the best possible decidability d' for BioBase data, and the optimal threshold $\tau^0_{\text{pers}} = 0.2185$.

To distinguish between relevant and irrelevant features within the final feature set $\mathbb{B}^*$, we introduce a set of masking bits, thus enlarging twice the required data for the iris template (we need to add 1024 bits to the existing set of 1024 bits representing iris features).

4. Iris Recognition System

4.1. Iris Template Creation

Image quality influences the reliability of the feature set. Consequently, a quality check is usually performed during enrollment which is slightly longer than the verification stage. We propose a two-stage procedure that leads to template internal consistency. This procedure has been applied in the prototype system. The first stage encompasses raw image quality check (calculation of the focus factor, eyelids/eyelashes coverage, identification of existence of specular reflections). After a successful check, eyeball rotation is corrected using correlation methods for all three images used for template creation. Since the aim is to enroll samples which are close in terms of the comparison score, the second stage investigates the consistency of acquired images as measured within the feature space. To check this, all possible comparisons are made between template feature sets. To pass the consistency check, all resulting scores should be lower than the acceptance threshold. We used thresholds established at the estimation stage (Subsecs. 3.6 and 3.7) as those values guarantee no sample errors, yet it is a choice of system administrator who may tune the template quality settings adequately to his needs. Consequently, as the iris template we select this feature set, for which the distance to the remaining feature sets is minimal (best candidate approach).

4.2. Eyeball Rotation Correction and Iris Verification

Small eyeball rotations in consecutive images may lead to considerable deterioration of within-eye comparison scores, Fig. 11. Since during verification the iris image corresponding to the template is unavailable, the rotation cannot be corrected by maximizing the correlation between the images and another methodology must be applied.

We use an iterative minimization of the comparison score between Zak-Gabor-based features determined for a set of small artificial shifts of the iris stripes being verified. This method is applied to both iris sectors independently, and the resulting codes corresponding to both sectors are compared separately. Obtained scores are averaged into the final score. However, correcting each incoming image is not reasonable, since a number of them do not require additional action, due to initial code robustness to eyeball slope. Thus, we apply a staged verification procedure that compensates for eye rotation only if necessary, i.e., if the comparison score does not drop below the acceptance threshold. Such an approach takes into account engineering aspects, since this minimizes the verification time. Approximately 55% of iris images in BioBase captured for verification do not require rotation correction for the threshold $\tau^0 = 0.3486$, and in the remaining genuine transactions we needed only 5 iterations (i.e., calculation of iris template for artificially shifted iris stripes) to find the best match.

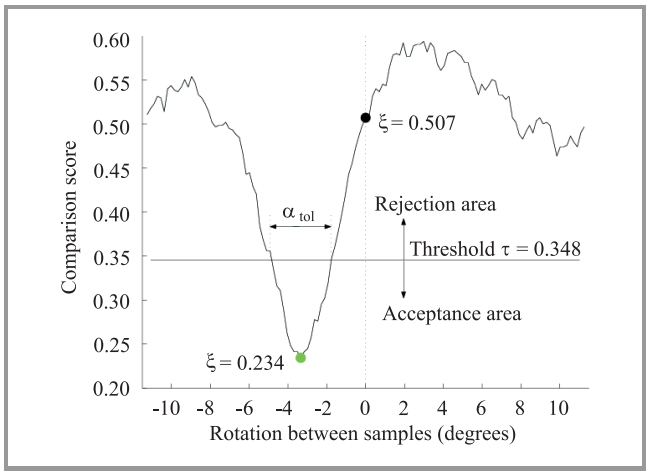

Fig. 11. Comparison score ξ vsersus mutual rotation angle α for two images of the same iris (results shown for one sector). Note that without rotation compensation, a non-match would be observed. The eye rotation tolerance α_{tol} (given the acceptance threshold) of a single code, illustrating its robustness to eyeball rotations is also marked; for BioBase data and the acceptance threshold $\tau^0 = 0.3486$ the average tolerance $\overline{\alpha}_{\text{tol}} \approx \pi/60$.

5. System Evaluation

5.1. Recognition Methodology Performance

For the purpose of evaluation, $N_g = K = 180$ genuine and $N_i = K(K-1)/2 = 32,220$ impostor comparisons were made, where $K = 180$ is the number of verification images, each representing different eye. Prior to the eyeball slope correction procedure, one should select the acceptance threshold τ^{rot}. Note that the thresholds $\tau^{\text{rot}} = 0.3486$

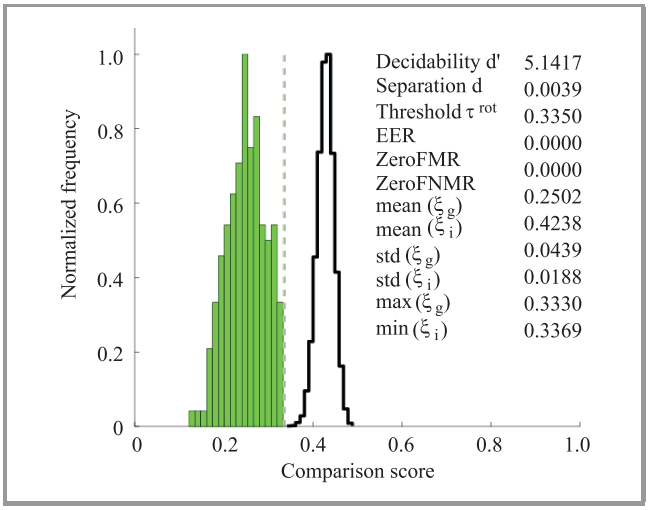

Fig. 12. Sample distributions of scores for non-personalized recognition method employing iterative minimization for eyeball slope correction. No sample errors were encountered for BioBase data and selected threshold $\tau^{\text{rot}} = 0.3350$.

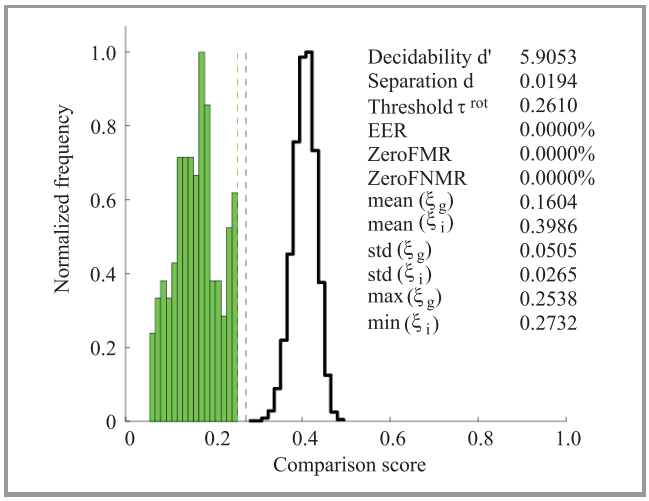

Fig. 13. Same as in Fig. 12, except the personalized recognition method is employed. No sample errors were encountered for BioBase data and selected threshold $\tau^{\text{rot}}_{\text{pers}} = 0.2610$.

used for Zak-Gabor-based coding for initially rotated samples (and $\tau^{\text{rot}}_{\text{pers}} = 0.2185$ when the personalized coding is used) are no longer valid, since the score calculation in this approach differs, i.e. it is iteratively minimized. Thus, to select the operating thresholds, full inspection is performed for all possible eyeball rotations and we set $\tau^{\text{rot}} = 0.3350$ and $\tau^{\text{rot}}_{\text{pers}} = 0.2610$ for non-personalized and personalized coding, respectively. No sample errors were encountered for BioBase data and selected thresholds, Figs. 12 and 13.

5.2. Operating Times

The methodology (and its variants) presented in the paper was implemented as the Software Development Kit [6] and was integrated with the IrisCUBE camera forming a standalone recognition system prototype. Current prototype is based on a PC workstation equipped with a 2.0 GHz Pentium processing unit, 1 GB RAM, controlled by Windows XP operating system, yet the system requirements guarantying reasonable processing times are much lower.

Table 1
Iris image acquisition and processing times achieved by the prototype system employing IrisCUBE camera, averaged for all BioBase acquisition sessions

Task	Average time [s]
Head positioning by skilled volunteer	2.5
Acquisition of frames	1.0
Best frame selection	1.5
Iris boundary localization and occlusions detection	0.8
Representation of iris image as a sequence of stripes	0.5
Zak-Gabor coefficients calculation and transformation into a features vector	0.05
Matching (with iterative minimization)	0.25
Total	6.6

Table 1 summarizes acquisition and processing times measured for all IrisCUBE acquisitions for BioBase. Although short training was offered to volunteers prior to data collection, the acquisition times are prone to relatively high uncertainty, due to the huge variability and unpredictability of human skills while positioning the subject's head. Processing times depend only on software implementation, hence the results may be predicted with a higher certainty in comparison to the volunteer behavior. The entire verification time, including the volunteer's mandatory cooperation and image acquisition, typically does not exceed 7 s, which is recognized by volunteers as an acceptable result.

6. Summary

The iris recognition project detailed in this paper encompasses the entire recognition system. We proposed a systematic approach of selection of the Zak-Gabor based coding parameters employing variance analysis of the iris features. The procedure allows selecting the frequency and scale of the image transformation appropriate in terms of the system reliability to the given iris image quality and resolution. This feature selection procedure can be applied also to other iris coding methods based on wavelet analysis. Presented methodology was used in a number of applications, for instance in remote access scenario and biometric smart card development. It was also evaluated in iris recognition system prototype with eye aliveness detection.

Acknowledgements

This paper has been financed by the Ministry of Science and Higher Education grant OR00 0026 07 "*A platform of secure biometrics implementations in personal verification and identification*".

References

[1] J. Daugman, "Biometric personal identification system based on iris analysis", *United States Patent* US 5,291,560, assignee: IriScan Inc., NJ, USA, March 1, 1994.

[2] A. Pacut and A. Czajka, "Aliveness detection for iris biometrics", in *Proc. 40th IEEE Int. Carnahan Conf. Secur. Technol. ICCST 2006*, Lexington, USA, 2006.

[3] *Information technology – Biometric data interchange formats – Part 6: Iris image data*, ISO/IEC International Standard 19794-6:2005(E)

[4] T. T. Chinen and T. R. Reed, "A performance analysis of fast gabor transform methods", *Graph. Mod. Image Proces.*, vol. 59, no. 3, pp. 117–127, 1997.

[5] M. J. Bastiaans, "Gabor's expansion and the zak transform for continuous-time and discrete-time signals", in *Signal and Image Representation in Combined Spaces*, J. Zeevi and R. Coifman, Eds. Academic Press, 1995, pp. 1–43.

[6] A. Czajka and A. Pacut, "BiomIrisSDK – software development kit for iris recognition", *NASK Review*, pp. 34–39, 2009.

Adam Czajka Adam Czajka received his M.Sc. in computer control systems in 2000 and Ph.D. in control and robotics in 2005 from Warsaw University of Technology, Poland. Since 2003 he is with Warsaw University of Technology, and since 2002 with Research and Academic Computer Network NASK working for Biometric Laboratories. He is a member of the NASK Research Council (2006–), NASK representative in Technical Committee No. 182 on Information Security in IT Systems (2007–) and in Technical Committee No. 309 on Biometrics (2010–) of Polish Committee for Standardization PKN. He is also a member of the IEEE (2002–) and recently served as the Secretary of the IEEE Poland Section (2006–2009).
e-mail: Adam.Czajka@nask.pl
Biometric Laboratories
Research and Academic Computer Network (NASK)
Wawozowa st 18
02-796 Warsaw, Poland

Andrzej Pacut holds Ph.D. in electronics and D.Sc. in control and robotics. Since 1969 he is with Warsaw University of Technology, being presently a professor and the head of Biometrics and Machine Learning Group in the Institute of Control and Computation Engineering. Since 2001 he is also the head of Biometric Laboratory of Research and Academic Computer Network NASK. He was Visiting Prof. in the Lefschetz Center for Dynamic Systems at Brown University, Providence, Rhode Island 1980–1981, and Visiting Prof. in the Department of Electrical and Computer Engineering of Oregon State University, Corvallis, Oregon, 1986–1991. He is a senior member of the IEEE and served as the Vice-Chair and then Chair of Poland Section of the IEEE in 2002–2009. He is the head of Technical Committee 309 on Biometrics of Polish Committee for Standardization PKN. He is interested in learning systems, biometrics, identification, bio-inspired modeling and control, and related areas.
e-mail: A.Pacut@ia.pw.edu.pl
Institute of Control and Computation Engineering
Warsaw University of Technology
Nowowiejska st 15/19
00-665 Warsaw, Poland

Biometric Laboratories
Research and Academic Computer Network NASK
Wąwozowa st 18
02-796 Warsaw, Poland